Separation Science and Technology
Publication details, including instructions for authors and subscription information:
http://www.informaworld.com/smpp/title~content=t713708471

Third-Phase Formation in the Extraction of Phosphotungstic Acid by TBP in *n*-Octane

Mark R. Antonio[a]; Renato Chiarizia[a]; Fanny Jaffrennou[§a]
[a] Chemical Sciences and Engineering Division, Argonne National Laboratory, Argonne, IL, USA

Online publication date: 30 August 2010

To cite this Article Antonio, Mark R. , Chiarizia, Renato and Jaffrennou[§], Fanny(2010) 'Third-Phase Formation in the Extraction of Phosphotungstic Acid by TBP in *n*-Octane', Separation Science and Technology, 45: 12, 1689 — 1698
To link to this Article: DOI: 10.1080/01496395.2010.493793
URL: http://dx.doi.org/10.1080/01496395.2010.493793

Separation Science and Technology, 45: 1689–1698, 2010

ISSN: 0149-6395 print/1520-5754 online
DOI: 10.1080/01496395.2010.493793

Taylor & Francis
Taylor & Francis Group

Third-Phase Formation in the Extraction of Phosphotungstic Acid by TBP in *n*-Octane

Mark R. Antonio, Renato Chiarizia, and Fanny Jaffrennou[§]
Chemical Sciences and Engineering Division, Argonne National Laboratory, Argonne, IL, USA

The solvent extraction of 12-phosphotungstic acid, also known as 12-tungstophosphoric acid—$H_3PW_{12}O_{40}$, the so-called Keggin heteropolyacid—by 0.73 M (20%v/v) tri-*n*-butyl phosphate (TBP) in *n*-octane under conditions comparable to those used previously for the extraction of conventional inorganic mineral acids is described. A simplified phase diagram for the pentanary system comprised of $H_3PW_{12}O_{40}$, HNO_3, H_2O, TBP, and *n*-octane reveals an extremely low initial concentration of $H_3PW_{12}O_{40}$ (1.1 mM) at the LOC (limiting organic concentration) condition, far lower than the most effective third-phase-forming inorganic acid, namely $HClO_4$. The results from small-angle neutron scattering (SANS) indicate that the interparticle attraction energy—$U(r)$ calculated through application of the Baxter sticky sphere model to the SANS data at the LOC condition—does not approach the $-2\ k_BT$ value associated with phase splitting in previous studies of TBP third-phase formation. The third-phase formation model based on attractive interactions between polar cores of reverse micelles, successfully developed for TBP and other extraction systems does not apply to the extraction of $H_3PW_{12}O_{40}$. Rather, the separation of a third-phase from the TBP organic phase stems from the limited solubility of the heavy and highly polar $H_3PW_{12}O_{40}$–TBP species in the alkane diluent.

Keywords Baxter model; heteropolyacid; Keggin ion; liquid-liquid extraction; polyoxometalate; small-angle neutron scattering

INTRODUCTION

One of the most troublesome phenomena in the extraction of nuclear materials by TBP (tri-*n*-butyl phosphate (TBP) depicted in Fig. 1a) is the formation of a third phase (1) wherein the organic phase splits into two layers—a light one composed mostly of the solvent and a heavy one (the so-called third phase) containing high concentrations of TBP and fissile materials (2–11). Although various strategies have been successfully employed to avoid the potentially catastrophic consequences of third-phase formation (12), despite more than 50 years of research, fundamental physico-chemical and structural aspects of the phenomenon remain to be completely understood.

The consensus of contemporary research (3,11–13) is that third-phase formation upon solvent extraction (SX) of metal salts and inorganic mineral acids (HNO_3, HCl, $HClO_4$, H_2SO_4, and H_3PO_4) by organic solutions of TBP is driven by the formation of reverse micelles in nonpolar diluents. These reverse micelles, which contain water and other polar solutes in their core domains, play a major factor in determining the propensity of the organic phase to split into two layers. Specifically, a recently developed model (3,7–11) demonstrates that organic phase splitting is due to van der Waals interactions between the polar cores of the reverse micelles. Small-angle neutron scattering (SANS) measurements illustrate that, independent of the chemical nature of the solutes—extractant and the extracted species alike—intermicellar attractions with energies of greater than $2k_BT$ (where k_B is the Boltzmann constant and T is temperature) are the prime operative forces in third-phase formation (3–11,14).

We wonder to what extent these results that stem from SX studies of simple metal nitrates and mineral acids apply to the extraction of complex, highly-charged heteropolyacids of which 12-phosphotungstic acid—$H_3PW_{12}O_{40}$, also known as 12-tungstophosphoric acid—is the archetype (15–17). In aqueous solutions of $H_3PW_{12}O_{40}$, the system properties vis-à-vis electroanalytical chemistry (18,19) and catalysis science (20) as well as the solute and solvent effects are predominantly the result of electrostatic interactions (21–23). The 12-phosphotungstic acid (abbreviated hereafter as HPT) with the α-Keggin structure (24,25) is the prototype of a large family of Brønsted acid salts of transition-metal oxoanions, known as polyoxometalate (POM) clusters, with the general composition $H_a[X_bM_cO_d]$, wherein X is typically a p-block ion, e.g., Al^{3+}, Si^{4+}, P^{5+}, and M is a d-block ion, e.g., Nb^{5+}, Mo^{6+}, W^{6+} (26,27). The HPT formula, $H_3PW_{12}O_{40}$, can be arranged in a number of different ways, including $H_3[P(W_3O_{10})_4]$ and $H_3[(PO_4)(W_{12}O_{36})]$. The latter description provides insight about its structure, which consists of a central PO_4 tetrahedral group surrounded by 12 WO_6 octahedral groups

Received 27 October 2009; accepted 17 March 2010.
[§]Student from INSA, Institut National des Sciences Appliquées de Rouen, France.
Address correspondence to Mark R. Antonio, Chemical Sciences and Engineering (CSE) Division, Argonne National Laboratory, Argonne, IL 60439, USA. E-mail: mantonio@anl.gov

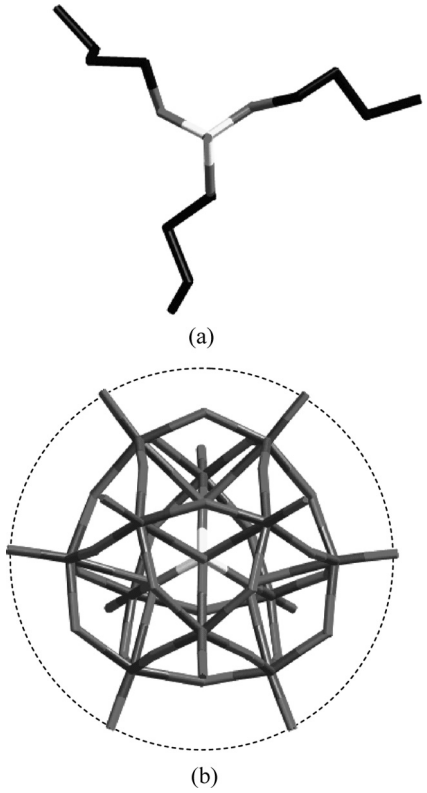

FIG. 1. Stick models drawn to scale of the molecular structures of (a, top) TBP, $(n\text{-}C_4H_9O)_3P{=}O$, in which the phosphoryl O atom is projecting outwards toward the reader and (b, bottom) $\alpha\text{-}[PW_{12}O_{40}]^{3-}$, where the dashed circle shows the crystallographic diameter of 10.4 Å.

as a shell, linked together by shared oxygen atoms as shown in Fig. 1b. In spite of the complexity of the molecule, the 53-atom, 12-phosphotungstic anion, $\alpha\text{-}[PW_{12}O_{40}]^{3-}$, is quite stable in aqueous acids and forms salts with practically all organic- and inorganic-cations (28). In fact, the insoluble ammonium salt of $\alpha\text{-}[PW_{12}O_{40}]^{3-}$ is of renown for its ion-exchange properties (28,29). These are common, collective properties of the series behavior of 12-heteropolyacids, including all X and M, and which have the effectively spherical structure (Fig. 1b) with an average crystallographic radius of 5.2 Å (21).

The results from experimental and theoretical studies alike (30,31) show that the 3 protons of HPT are located on three of the twelve terminal O atoms that form the short W=O bonds at a distance of 5.7 ± 0.2 Å from the central P^{5+} ion. With regard to the acidity of HPT, the general literature indicates that it fits in with the strongest mineral acids and, in the solid state, it is oftentimes compared with the so-called superacids (32–34). Indeed, with its 1.60, 3.54, and 7.16 pK_a values, $H_3PW_{12}O_{40}$ is of an acidity comparable to that of ordinary mineral acids or corresponding oxoacids arising from any combination of its constituent elements (35). Therefore, the extraction of HPT by TBP described here is readily compared with the latest SX results obtained for the acids of common inorganic oxoanions—NO_3^-, ClO_4^-, SO_4^{2-}, and PO_4^{3-} (2).

A three-part series of historical and encyclopedic articles by Lakshmanan and Haldar (36–38) from four decades ago have shown that 12-heteropolyacids, including $H_3PMo_{12}O_{40}$, $H_3PW_{12}O_{40}$, $H_4SiMo_{12}O_{40}$, and $H_4SiW_{12}O_{40}$, can be extracted into neat, oxygenated organic solvents in the form of solvated ion pairs and that this phenomenon is profoundly influenced by the basicity and dielectric constant of organic solvents (36,37). The extraction of the same four heteropolyacids by TBP in benzene and nitrobenzene provides evidence that three molecules of TBP are associated with each acid in the organic phases (38). No organic phase splitting was reported and, also, in more recent studies by Asakura et al. (39) with a selection of three different heteropolyanions—$[P_2W_{18}O_{62}]^{6-}$, $[P_2W_{17}O_{61}]^{10-}$, and $[SiW_{11}O_{39}]^{8-}$—all of greater acidity and charge than HPT, no third-phase formation was reported upon their extraction with 30% (v/v) TBP in *n*-dodecane.

In order to address the organic phase splitting issues with attention to conditions of relevance to practical SX processes today, which employ aliphatic diluents and aqueous nitric acid media of 3 M (or more) concentration, and to determine at what level parallels can be drawn with the trends in third-phase formation behavior observed with the simple oxoanions of mineral acids, we have investigated the extraction of HPT by 20% (v/v) TBP solutions in *n*-octane at various HPT concentrations and constant temperature. The objective was to determine the critical point of third-phase formation (known as the limiting organic concentration, LOC, of the extracted species), and whether it takes place according to the mechanism of van der Waals attraction between reverse micelles. Going into this study, it was our hypothesis that below a critical, limiting concentration, HPT may exhibit a random and homogeneous distribution in TBP, free of both solute and solvent effects. Similarly, above a critical HPT concentration, ion pairing and other electrostatic associations leading to aggregation are expected to affect the bulk physical and structural responses of the solution in ways that may be different from the general reverse micelle interaction model. As such, we have elucidated the correlation effects that drive solution structures in the HPT SX system by use of small-angle neutron scattering (SANS).

EXPERIMENTS

Materials

$H_3PW_{12}O_{40} \cdot nH_2O$ from Aldrich Chemicals was used without further purification. The ^{31}P NMR response showed a single line at -14.6 ppm, consistent with the α-isomer (40), and the mass fraction of water (12.24%) was determined from quantitative analysis of the NMR with a calibration standard of 50 μL 0.991 M H_3PO_4 in

1 mL D_2O. *n*-Octane and deuterated *n*-octane (d_{18}, 98 atom % D) were obtained from Aldrich Chemicals. All other reagents were the same as used beforehand (2).

Procedures and Analyses

Extraction Experiments

In each of the four liquid-liquid extraction experiments, the organic phase was composed of 0.73 M TBP (20%v/v) in *n*-octane and the aqueous phase consisted of $H_3PW_{12}O_{40}$ at four concentrations in 0.984 M nitric acid. It must be noted that when HPT is extracted from distilled, deionized water (17.9 MΩ cm), a white interfacial crud forms immediately upon contact with the TBP-containing organic phase. Although the composition of this precipitate is unknown, the sensitivities of this heteropolyacid to neutral and alkaline media are well known (41), and the white precipitate may well be a number of W-containing species resulting from the hydrolytic damage of the α-Keggin framework structure (Fig. 1b) of HPT. For this reason, the extraction of HPT was performed in the presence of 0.984 M HNO_3. Four concentrations of HPT were prepared, including two pre-LOC conditions, one for the LOC condition and one for the post-LOC condition. Equal volumes of aqueous and organic phases were used (4–5 mL) for the liquid-liquid extraction. The biphasic media, contained in glass, screw-cap test tubes, were equilibrated at 25 ± 0.5°C in a water bath followed by random-orbit vortexing for about 1 hour, followed by re-immersion and re-equilibration in the 25°C water bath. This procedure was repeated three times. After the final cycle, the samples were centrifuged and aliquots of the equilibrium phases subjected to physical analyses as well as chemical analyses of the constituent compositions in the pentanary system $H_3[PW_{12}O_{40}]$-HNO_3-H_2O-TBP-*n*-C_8H_{18}. For the determination of the LOC condition, the same procedure was used as previously reported (2).

Acid Concentration

The aqueous phases were titrated potentiometrically using 1 M NaOH standard solutions. The organic phases were stripped three times with 2 mL of water and the combined strip solutions were titrated in the same way, but using a 0.1 M NaOH standard solution. A full and complete strip of HPT from the third-phase was impossible to achieve. Even after contacting ~2 mL of third-phase with many aliquots of 0.1 M HNO_3 (for a total of 110 mL), a drop of third-phase still remained. Moreover, the acid-base titrations of all HPT-containing aqueous solutions could not be performed up to the neutral end-point because decomposition of the P-W-O anion was observed to commence at pH values as low as 3 (41). Therefore, the titrations were cut short at pH values slightly lower than 3. This introduced a small error in the results of the titrations.

Water Concentration

Water in the organic phases was determined by Karl Fisher titrations using $H_2C_2O_4 \cdot 2H_2O$ as the standard.

TBP Concentration

In the three samples where no third-phase was generated, the equilibrium TBP concentration was assumed to be equal to the initial concentration, i.e., 0.73 M, neglecting small changes of the organic phase volume upon extraction of acid and water. The TBP concentrations in the heavy and light organic phases resulting from phase splitting were determined from the distribution ratio (D) of ^{233}U (from ANL stocks, purified from ^{229}Th and daughters using the UTEVA resin) (42) between the organic phase samples and 3 M HNO_3 by using a calibration curve of D_U vs TBP concentration.

Tungsten Concentration

All solutions containing HPT were submitted for quantitative analyses of tungsten by ICP-AES analyses, which proved problematic in two regards:

(1) high variance between replicate measurements, and
(2) increasing background signals.

These vitiating behaviors could not be mitigated by dilution, indicating that it was not possible to get the analyte cleanly into the plasma because the tungsten-bearing molecular anion interacted strongly with surfaces in the sample introduction system of the ICP apparatus. Therefore, a ±20% uncertainty was assigned to the results. In view of the difficulties and uncertainties with ICP analyses, an alternate, electroanalytical approach to obtain additional quantitative information about the HPT solution concentrations was conceived. Remarkably, this approach, too, presented insuperable problems because the HPT concentrations in the strip solutions were below the limit of detection of the method.

Small-Angle Neutron Scattering

The SANS measurements were performed at the time-of-flight small-angle diffractometer (43) at the Intense Pulsed Neutron Source, which has since been decommissioned. The samples were measured in standard Suprasil cells with a pathlength of 2 mm, a sample volume of 0.8 mL, and data collection time of three hours. For each sample, the data were collected as scattered intensity $I(Q)$ (cm^{-1}) vs. momentum transfer ($Q = (4\pi/\lambda)\ \sin(\theta)$ ($Å^{-1}$)), where θ is half the scattering angle and λ is the wavelength of the probing neutrons. The absolute intensity of the scattering data was obtained using secondary standards of polymer and porous silica with known cross sections, following the procedure reported previously (43). For the interpretation of the SANS data, the following equation

describing scattering by a monodisperse system of particles was used:

$$I(Q) = N_p V_p^2 (\rho_p - \rho_s)^2 P(Q) S(Q) + I_{inc} \quad (1)$$

Here $I(Q)$ is the intensity of the neutrons scattered by the solute particles (obtained from the experimental intensities by subtracting the intensities measured for the diluent alone); N_p is the number of scattering units per unit volume; V_p is the particle volume; $(\rho_p - \rho_s)^2$ is the contrast factor (determined by the difference in the neutron scattering length density of particles and solvent); $P(Q)$ is the single particle form factor, which describes the angular scattering distribution as a function of particle size and shape; $S(Q)$ is the structure factor, which accounts for interactions between the scattering particles; and I_{inc} is the incoherent scattering background (44).

RESULTS AND DISCUSSION

Phase Behavior

The distribution isotherms for each of the four solutes—$H_3PW_{12}O_{40}$-TBP-HNO_3-H_2O—in the organic phases of the *n*-C_8H_{18} solvent system were prepared from the assortment of analytical data, including titrimetry, spectrometry, D_U, and mass balance considerations. For example, the ICP analyses of tungsten in the equilibrium aqueous phases for the three experiments where the initial HPT concentrations were 6×10^{-4}, 9×10^{-4}, and 1.1×10^{-3} M (LOC condition), showed that the concentrations of residual HPT in the aqueous phase was below the detection limit of ca. 2×10^{-6} M. This demonstrates that the extraction of HPT by TBP is effectively quantitative.

For the system where a third-phase was present (with an initial HPT concentration of 0.01 M), the HPT concentration in the middle aqueous phase was 2.26×10^{-6} M. However, the results of the ICP analyses for the solutions obtained from stripping HPT from the light (top) and the heavy (bottom) phases were much too low to be realistic. Besides the previously discussed difficulties with the ICP analysis of the heteropolyacid, the major problem here is that, as mentioned earlier, the strip of HPT from the TBP organic phase with 0.1 M HNO_3 was far from quantitative. Stripping with water would have been more effective, but was not an option as it leads to decomposition of the P-W-O structure of the molecular anion and precipitates. So, based on the analogy with other third-phase systems where the solute concentration in the light phase is typically slightly lower than that at the LOC condition (2,14), it was assumed that the HPT concentration in the light phase was 8×10^{-4} M, i.e., slightly lower than the 1.1×10^{-3} M of the LOC point. Having measured as precisely as possible the volumes of the three phases in equilibrium (eq) (e.g., 8.00 mL of initial aqueous (aq) and organic phases generated, after equilibration, 7.95, 7.60, and 0.45 mL of aqueous, light, and heavy (h) phases, respectively), a mass balance relation was used to calculate the HPT concentration in the heavy phase as follows:

$$[HPT]_{aq,init} \times V_{aq,init} = [HPT]_{aq,eq} \times V_{aq,eq} + [HPT]_{light,eq} \times V_{light,eq} + [HPT]_{h,eq} \times V_{h,eq} \quad (2)$$

In this manner, the HPT concentration in the heavy phase was calculated as 0.15 M. Table 1 collects all the analytical data obtained on the HPT–0.73 M TBP–*n*-octane system.

The results in Table 1 were used to draw the simplified phase diagram shown in Fig. 2, in which the point corresponding to the HPT limiting organic concentration, LOC, is easily identified by the intersection of the three curves describing the HPT, HNO_3, H_2O, and TBP concentrations in the biphasic and triphasic regions of the diagram. When a 0.73 M TBP solution in *n*-octane is equilibrated with an aqueous phase having a HPT concentration higher than that corresponding to the LOC condition, the organic phase splits into two layers. The HPT concentrations in the two organic phases resulting from

TABLE 1
Compositions and concentrations (in M) of the constituent species in the organic phases at equilibrium for the HPT-HNO_3-TBP-*n*-octane system at 25 ± 0.5°C

Sample ID	$[HPT]_{init,aq}$[a]	[HPT][b]	$[HNO_3]$[b]	$[H_2O]$[b]	[TBP][b]
Blank	–	–	–	0.21	0.73
Pre-LOC(1)	0.0006	0.0006	0.11	0.21	0.73
Pre-LOC(2)	0.0009	0.0009	0.11	0.21	0.73
LOC	0.0011	0.0011	0.11	0.21	0.73
Light phase	0.01	0.0008	0.086	0.16	0.39
Heavy phase	0.01	0.15	0.12	2.0	1.50

[a]In 0.984 M HNO_3.
[b]Uncertainty intervals: ±20% for [HPT], ±5% for $[HNO_3]$, ±10% for $[H_2O]$, and ±5% for TBP.

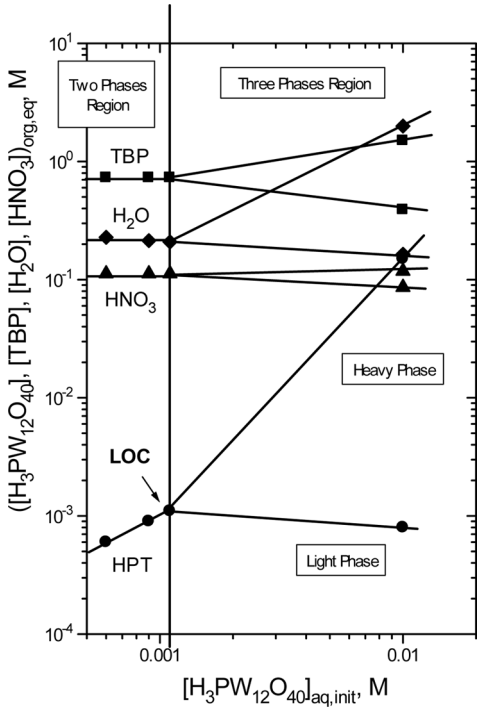

FIG. 2. Simplified phase diagram for the extraction of HPT by 0.73 M TBP in *n*-octane at 25 ± 0.5°C.

third-phase formation are described by the lines in the triphasic regions of Fig. 2. All the solutes in the organic phase (HPT, HNO_3, TBP, and H_2O) distribute asymmetrically between the light and heavy organic phases, reporting mostly in the heavy layer, whereas the light organic phase is a diluted solution of the various solutes. It is interesting to note that the concentration of both TBP and water in the third-phase approaches the 2 M level, a result consistent with the third phase formed in the extraction of inorganic acids (2).

The most striking feature of the data in Fig. 2 however, is the extremely low initial concentration of HPT at the LOC condition, far lower than the most effective third-phase forming inorganic acid, namely perchloric acid (2). The third phase formed in a system where the HPT concentration is slightly higher than that corresponding to the LOC point, consists of a very small, clear, colorless drop with a diameter of ~2 mm that forms at the bottom of the test tube. The phenomenon is reversible and reproducible and undoubtedly represents third-phase formation. A striking aspect of this system is that the third phase is physically below the aqueous phase. In contrast, third phases formed upon extraction of mineral acids under the same conditions separate the light organic phase, which is at the top, from the aqueous phase, which is at the bottom. As far as we know, the HPT-containing third phase is unique in being denser than water, $\rho = 1.28\ \mathrm{g\,mL^{-1}}$.

SANS

SANS measurements were performed for the same samples as in Table 1, the only difference being that deuterated *n*-octane was used as the diluent for TBP. The data for the HPT-free blank, the pre-LOC(2) and the LOC sample are shown in Fig. 3. The scattering intensities in Fig. 3 are very low and the $I(Q)$ data for the pre-LOC and LOC samples are nearly coincident with the blank sample. Therefore the initial inspection of the SANS data suggests little or no aggregation of the TBP species formed upon extraction of HPT at and before its LOC condition beyond that which obtains for the HPT-free system. In other words, HPT appears to be precisely accommodated within the core of the reverse micelles without significant morphological perturbation.

The SANS results for the light and heavy phase samples are shown in Fig. 4 where they are compared with those for the blank sample. As expected, the light phase sample, which contains very low concentrations of the inorganic solutes and a lower TBP concentration (0.39 M) than the blank (0.73 M), exhibits extremely low scattering intensities that are even lower than that of the blank sample. In contrast, stronger scattering is given by the third-phase sample, which is a much more concentrated solution of TBP and polar solutes. Compared to the other samples, the scattering signals suggest increased average size and interaction for the particles present in the third-phase sample.

The SANS data of Figs. 3 and 4 were interpreted using the same approach developed and successfully applied for the extraction of HCl (3,8,9) and other inorganic mineral acids by TBP in aliphatic diluents. In this way, the results of the present investigation can be compared directly with

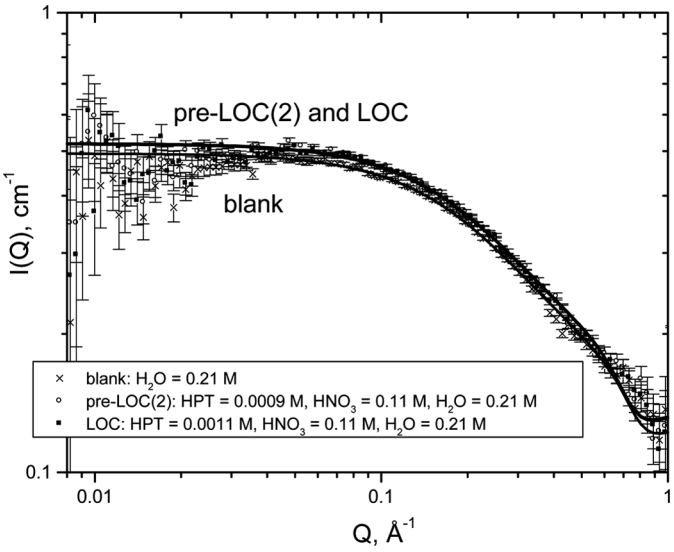

FIG. 3. SANS data and Baxter model fits for blank, pre-LOC(2), and LOC samples.

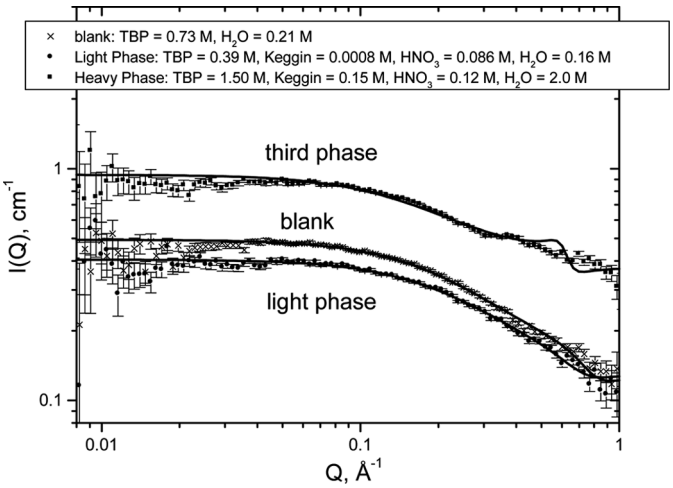

FIG. 4. SANS data and Baxter model fits for blank, light phase, and third-phase samples.

those for the systems investigated earlier. In this approach we used the Baxter model for hard spheres with surface adhesion (also known as the "sticky spheres" model) as described elsewhere (45). According to this model, the hard sphere sticky potential, $U(r)$ expressed in k_BT units as a function of interparticle distance (r), and the stickiness parameter (τ^{-1}) are high for strong interaction between particles and low for weak interactions. Another useful feature of Baxter's model approximation is that analytical expressions have been derived for the structure factor $S(Q)$ of Eq. (1) (46,47). In combination with the expression for a spherical form factor $P(Q)$ (44), three parameters, I_{inc}, d_{hs}, and τ, were used to best fit the SANS data, where d_{hs} is the hard sphere particle diameter, i.e., the distance below which the particles are incompressible.

To accomplish this, the solute volume fractions were calculated from the solute concentrations in Table 1. The molar volumes of H_2O, HNO_3, the polar head of TBP, and the nonpolar portion of TBP were taken from previous work (3); that of HPT was calculated using a density value of $5.31\,g\,mL^{-1}$ which, in turn, was derived from structural data (25). The contrast factor for each solute was calculated by using the scattering length densities of the solutes and of deuterated octane. For each sample, the total contrast factor was obtained from the contrast factor of each solute in the sample by summing the contribution of each solute in proportion to its molar concentration. Table 2 contains the values of I_{inc}, d_{hs}, and τ^{-1} provided by the Baxter model fits (shown as solid lines) to the experimental data of Figs. 3 and 4. As an example of deconstruction of the modeling procedure, the experimental data for the HPT third phase are shown in Fig. 5 along with the best fit $S(Q)$, $I(Q)$ and $P(Q)$ curves. The $S(Q)$ curve exhibits a strong correlation peak at $Q = 0.63\,Å^{-1}$, which was used to obtain the correlation distance between interacting particles through Bragg's law in the form $d = 2\pi/Q$.

For each sample, the weight-average volume of the hard sphere, V_{hs}, was also calculated using the value of d_{hs}:

$$V_{hs} = \frac{1}{6}\pi d_{hs}^3 \tag{3}$$

This volume comprises both the volume of the hydrophilic constituents of the particle core structure (which contains H_2O, HNO_3, $H_3PW_{12}O_{40}$, and the $-O_3P{=}O$ groups of the TBP molecules) and the volume occupied by the n-butyl chains of TBP (the lipophilic corona). By using the analytical data in Table 1, the volume of the polar micellar core

TABLE 2
Results obtained from the best fits of the SANS data ($0.01 \le Q \le 1.0\,Å^{-1}$) of the organic phases (in deuterated n-octane at $25 \pm 0.5°C$) using the Baxter model

Sample ID	I_{inc}[a] cm^{-1}	d_{hs}[b] Å	Correlation peak[c] Å	d_p[d] Å	t_c[e] Å	$n_{w,av}$[f] TBP	$1/\tau$[g]	$U(r)$[h] k_BT
Blank	0.12	9.7	7.8	5.8	2.0	1.0	5.0	−1.4
Pre-LOC(2)	0.13	10.2	8.6	6.3	2.0	1.2	4.9	−1.4
LOC	0.13	10.2	8.6	6.3	2.0	1.2	4.9	−1.4
Light phase	0.12	10.5	8.8	6.6	2.0	1.2	4.9	−1.4
Heavy phase	0.36	12.5	10.0	9.1	1.7	1.7	28	−3.2

[a]Incoherent scattering; uncertainty ±1%.
[b]Hard sphere diameter; uncertainty ±10%.
[c]From $S(Q)$ vs. Q plots like Fig. 5; uncertainty ±10%.
[d]Polar core diameter; uncertainty ±10%.
[e]Corona thickness; uncertainty ±10%.
[f]Weight-average aggregation number; uncertainty ±10%.
[g]Stickiness parameter; uncertainty ±5%.
[h]Energy of attraction between particles; uncertainty ±5%.

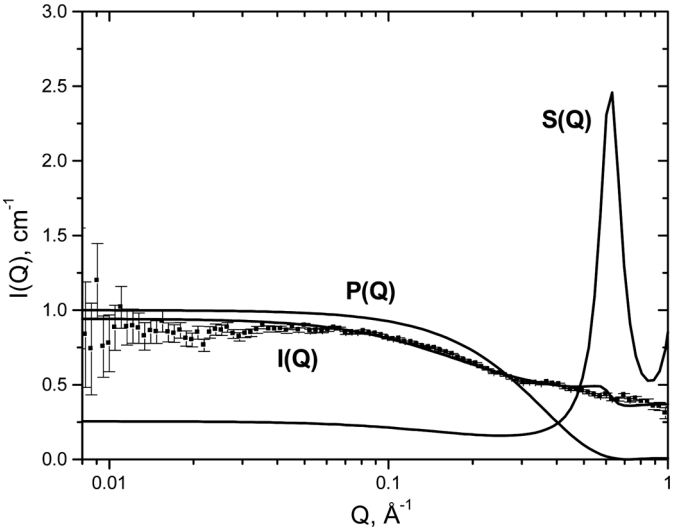

FIG. 5. Experimental SANS data and calculated curves for $I(Q)$, $P(Q)$, and $S(Q)$ for the dense third phase.

and, hence, its weight-average diameter (d_p in Table 2) was calculated by multiplying the total volume of the micelle by the ratio of polar solutes to total solutes volume fraction. The volume of the corona was then estimated by subtracting the volume of the polar core from the total micellar volume, and the corona thickness (t_c in Table 2) was obtained from d_{hs} and the diameter of the polar core. Finally, the weight-average aggregation number of TBP in the micelle, $n_{w,av}$ in Table 2, was obtained by dividing the volume of the corona by the nonpolar volume of TBP.

From the τ values provided by the Baxter fit of the SANS data, the attractive potential energy between two particles, $U(r)$ in k_BT units, was calculated assuming an attractive well width equal to 10% of the hard sphere diameter (3,9,14). The $U(r)$ values are also reported in Table 2.

Based on the d_{hs} values from the SANS data, it appears that the scattering particles with HPT are small (10.2–10.5 Å) and their size is statistically equivalent to the blank system, 9.7 Å. The significant exception is with the third phase, which exhibits a 2 Å larger d_{hs}. Coincidentally, the values of the weight-average aggregation numbers of TBP for the HPT solutions (1.2) are indistinguishable from that (1.0) for the blank. The exception is for the third phase for which a value of 1.7 is obtained. As such, there is no significant solute aggregation in the systems investigated at the LOC (and lower) concentrations of HPT. The solutes are mostly TBP monomers in equilibrium with a small number of molecular HPT entities containing one TBP molecule hydrogen bonded to the extracted HPT. Because all the SANS metrical results in Table 2 are values that are weight-averaged over all the particles in solutions, including TBP monomers, it is not surprising that the weight-average diameter of the polar core for the various samples is always smaller than the crystallographic diameter of HTP (10.4 Å) (21).

From the $n_{w,av}$ obtained for the third-phase sample it was possible to calculate the number of TBP molecules solvated to the HPT species in equilibrium with the TBP monomers by using the equation that relates the weight-average aggregation number to the real aggregation numbers of the single species present in the solution (48):

$$n_{w,av} = \frac{\sum_i n_i^2 C_{aggr,i}}{\sum_i n_i C_{aggr,i}} \quad (4)$$

Here, n_i and $C_{aggr,i}$ are the aggregation number and concentration of each aggregate. By assuming that the total TBP concentration of 1.5 M is distributed between monomers and 0.15 M (the HPT concentration) aggregates containing n TBP molecules, the following relations hold:

$$1.73 = \frac{[TBP]_{mon} + 0.15n^2}{[TBP]_{mon} + 0.15n} \quad (5)$$

where $[TBP]_{mon}$, the concentration of free monomeric TBP, is given by:

$$[TBP]_{mon} = 1.5 - 0.15n \quad (6)$$

Equations (5) and (6) were resolved for $[TBP]_{mon}$ and n by computer iterations to provide an n value of 3.2. This value of n, close to 3, indicates that in the HPT-TBP species in the third phase each H atom of HPT is hydrogen bonded to a TBP molecule, thus confirming previous literature results from SX studies with non-aliphatic diluents (38).

The $H_3PW_{12}O_{40} \cdot (TBP)_3$ species in the heavy phase interact strongly with each other, as indicated by the very high stickiness parameter (28.4) and attraction energy ($-3.2\ k_BT$). For all other samples in Table 2, especially the LOC condition, both the stickiness parameters and attraction energies are very low and indistinguishable from the blank sample. The values of $U(r)$ are constant ($-1.4\ k_BT$) with varying [HPT] right up to the LOC condition and never approach the $-2\ k_BT$ level, which was found to be associated with phase splitting in previous studies on TBP third-phase formation (3,5–11).

Both the sharp correlation peak in the *S(Q)* plot in Fig. 5 and the high potential energy of interparticle attraction suggest that the third phase is a structured solution. The large number of electron-rich atoms in the polar core of the reverse micelles make the system an ideal candidate for structural investigations using X-ray based techniques, such as, small-angle X-ray scattering (SAXS) and high-energy X-ray scattering (HEXS). The results of these investigations will be discussed in a future communication together with the electrochemical behavior of $H_3PW_{12}O_{40}$ in the *n*-octane-TBP organic phase.

The phase-splitting behavior with HPT is unique, and stands in contrast with that for the inorganic mineral acids, wherein the splitting is directly correlated with an increase of the attraction energy between solute particles. Based on the results from the SANS measurements, we conclude that the third-phase formation model founded on attractive interactions between polar cores of reverse micelles, successfully developed for other TBP extraction systems, does not apply to the extraction of HPT. Instead, the separation of a very heavy phase from the TBP original organic phase is attributed to the miniscule solubility of the heavy and highly polar $H_3PW_{12}O_{40} \cdot (TBP)_3$ species in the *n*-octane diluent. This result, however, is not completely unexpected. A species with the $H_3PW_{12}O_{40} \cdot (TBP)_3$ composition is made of 71 hydrophilic atoms vs only 36 carbon atoms in the lipophilic chains. The expectation of high solubility of this species in an *n*-alkane diluent would be unrealistic. Then again, a much higher solubility of the HPT-extractant species would be expected if the extractant had much longer alkyl chains. The more lipophilic species formed in this case may still follow the general micellar mechanism for third-phase formation outlined above.

Besides the obvious connection with SX, the formation of $H_3PW_{12}O_{40} \cdot (TBP)_3$ and its characterization, resulting in the idealized morphology depicted in Fig. 6, is of contemporary interest, both practical and fundamental, vis-à-vis the new class of deliberately-formed, surfactant-encapsulated POMs (49–56) as well as the chemistry of structured fluids. The liquid-liquid extraction procedure provides a new entry to the preparative chemistry of extractant-encapsulated systems with other heteropolyacids, including the eponymous Wells-Dawson $[P_2M_{18}O_{62}]^{6-}$ (for $M \equiv Mo^{6+}$ and W^{6+}) and Preyssler $[M^{n+}P_5W_{30}O_{110}]^{(n-15)}$ (for $M \equiv Na^+$, Ca^{2+}, Sr^{2+}, Y^{3+}, La—Lu^{3+}, Th^{4+}, U^{4+}, Pu^{3+}—Cm^{3+}) polyoxoanions, to name just two, as well as their lacunary species (27). Based upon the research reported herein, which describes the preparation and selected physical properties of a Keggin heteropolyacid-containing third phase, the numerous other POM systems are likely to exhibit third-phase behaviors too. Details of the colligative properties and morphological relationships between heteropolyacids and neutral extractants of variable surface active properties and between POMs and neutral as well as ionic surfactants prepared by conventional synthetic means remain to be understood and, ultimately, controlled for prospective applications in catalysis and separation sciences.

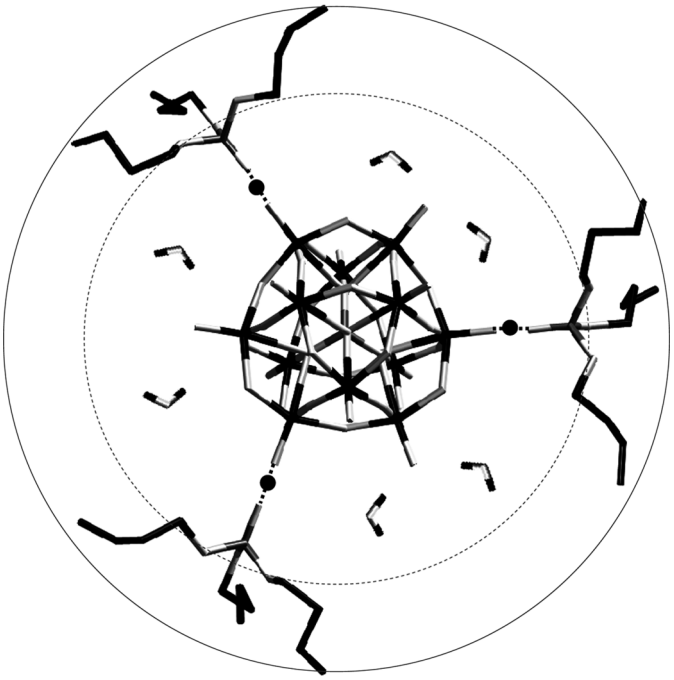

FIG. 6. Idealized illustration of the $H_3PW_{12}O_{40} \cdot (TBP)_3$ solvate in the third phase. HPT is contained within the hydrophilic polar core (with the diameter designated by the inner, dashed circle) of the reverse micelle. The hydrogen bonding between the phosphoryl O atom and the terminal O atom of α-$[PW_{12}O_{40}]^{3-}$ occurs through the three protons (black circles) of the HPT. The micelle diameter is depicted with the solid circle, and the area between it and the inner dashed circle represents the lipophilic corona thickness.

CONCLUSIONS

The extraction of $H_3PW_{12}O_{40}$ presented unexpected experimental difficulties due to a number of factors, such as the tendency of HPT to decompose when it is not in strongly acidic media and the limited reliability of the tungsten analysis by ICP-AES. Nevertheless, by use of reasonable approximations and mass balance equations, it was possible to establish a simplified phase diagram for the system comprised of $H_3PW_{12}O_{40}$, HNO_3, H_2O, TBP, and *n*-octane. The most striking feature of this phase diagram is the extremely low initial concentration of HPT at the LOC condition (1.1 mM), far lower than the most effective third-phase forming inorganic acid, namely $HClO_4$. SANS data indicated that the scattering particles are small and their size is only modestly associated with sample composition. The values of the weight-average aggregation numbers of TBP are always close to one, except for the HPT third-phase sample, suggesting that little or no solute aggregation takes place in the systems investigated. The solutes in these organic solutions are TBP monomers in equilibrium with species containing only one (two at most) TBP molecule(s) hydrogen bonded to the extracted HPT. However, analysis of the SANS data revealed the presence of strongly interacting $H_3PW_{12}O_{40} \cdot (TBP)_3$ trisolvate species in the highly structured heavy phase formed upon extraction of HPT. The values of interparticle attraction energy, $U(r)$, calculated through the application of the Baxter sticky sphere model to the SANS data at the LOC condition, never approached the $-2\ k_BT$ level associated with phase splitting in previous studies on TBP third-phase formation. The third-phase formation model based on

attractive interaction between the polar cores of reverse micelles, successfully developed for other TBP extraction systems does not apply to the extraction of HPT. Rather, the separation of a third phase from the original TBP organic phase stems from the limited solubility of the heavy and highly polar $H_3PW_{12}O_{40} \cdot (TBP)_3$ solvate in the alkane diluent.

NOTE BY AUTHOR(S)

ACKNOWLEDGEMENTS

We thank Paul Rickert and Denis Wozniak for assistance with the NMR and SANS measurements. This work was supported by the U.S. Department of Energy, Office of Basic Energy Science, Division of Chemical Sciences, Biosciences and Geosciences, under contract No. DE-AC02-06CH11357.

REFERENCES

1. Naylor, A.; Wilson, P.D. (1983) Recovery of uranium and plutonium from irradiated nuclear fuel. In: *Handbook of Solvent Extraction*, Lo, T.C.; Baird, M.H.I.; Hanson, C., eds.; Wiley: New York, 783–798.
2. Chiarizia, R.; Briand, A. (2007) Third phase formation in the extraction of inorganic acids by TBP in *n*-octane. *Solvent Extr. Ion Exch.*, 25: 351–371.
3. Chiarizia, R.; Briand, A.; Jensen, M.P.; Thiyagarajan, P. (2008) SANS study of reverse micelles formed upon the extraction of inorganic acids by TBP in *n*-octane. *Solvent Extr. Ion Exch.*, 26: 333–359.
4. Chiarizia, R.; Jensen, M.P.; Borkowski, M.; Ferraro, J.R.; Thiyagarajan, P.; Littrell, K.C. (2003) Third phase formation revisited: The U(VI), HNO_3-TBP, *n*-dodecane system. *Solvent Extr. Ion Exch.*, 21: 1–27.
5. Chiarizia, R.; Jensen, M.P.; Borkowski, M.; Thiyagarajan, P.; Littrell, K.C. (2004) Interpretation of third phase formation in the Th(IV)-HNO_3, TBP-*n*-octane system with Baxter's ''sticky spheres'' model. *Solvent Extr. Ion Exch.*, 22: 325–351.
6. Chiarizia, R.; Jensen, M.P.; Rickert, P.G.; Kolarik, Z.; Borkowski, M.; Thiyagarajan, P. (2004) Extraction of zirconium nitrate by TBP in *n*-octane: Influence of cation type on third phase formation according to the ''sticky spheres'' model. *Langmuir*, 20: 10798–10808.
7. Chiarizia, R.; Nash, K.L.; Jensen, M.P.; Thiyagarajan, P.; Littrell, K.C. (2003) Application of the Baxter model for hard spheres with surface adhesion to SANS data for the U(VI)-HNO_3, TBP-*n*-dodecane system. *Langmuir*, 19: 9592–9599.
8. Chiarizia, R.; Rickert, P.G.; Stepinski, D.; Thiyagarajan, P.; Littrell, K.C. (2006) SANS study of third phase formation in the HCl-TBP-*n*-octane system. *Solvent Extr. Ion Exch.*, 24: 125–148.
9. Chiarizia, R.; Stepinski, D.C.; Thiyagarajan, P. (2006) SANS study of third phase formation in the extraction of HCl by TBP isomers in *n*-octane. *Sep. Sci. Technol.*, 41: 2075–2095.
10. Nave, S.; Mandin, C.; Martinet, L.; Berthon, L.; Testard, F.; Madic, C.; Zemb, T. (2004) Supramolecular organisation of tri-*n*-butyl phosphate in organic diluent on approaching third phase transition. *Phys. Chem. Chem. Phys.*, 6: 799–808.
11. Plaue, J.; Gelis, A.; Czerwinski, K.; Thiyagarajan, P.; Chiarizia, R. (2006) Small-angle neutron scattering study of plutonium third phase formation in 30% TBP/HNO_3/alkane diluent systems. *Solvent Extr. Ion Exch.*, 24: 283–298.
12. Rao, P.R.V.; Kolarik, Z. (1996) A review of third phase formation in extraction of actinides by neutral organophosphorus extractants. *Solvent Extr. Ion Exch.*, 14: 955–993.
13. Pugaev, D.V.; Sinegribova, O.A. (2007) Tri-*n*-butyl phosphate-decane-mineral acid three-phase systems. *Russ. J. Inorg. Chem.*, 52: 1140–1143.
14. Chiarizia, R.; Stepinski, D.; Antonio, M.R. (2010) SANS study of HCl extraction by selected neutral organophsphorus compounds in *n*-octane. *Sep. Sci. Technol.* this volume.
15. Micek-Ilnicka, A. (2009) The role of water in the catalysis on solid heteropolyacids. *J. Mol. Catal. A-Chem.*, 308: 1–14.
16. Timofeeva, M.N. (2003) Acid catalysis by heteropoly acids. *Appl. Catal. A-Gen.*, 256: 19–35.
17. Kozhevnikov, I.V. (1998) Catalysis by heteropoly acids and multicomponent polyoxometalates in liquid-phase reactions. *Chem. Rev. (Washington, D.C.)*, 98: 171–198.
18. Sadakane, M.; Steckhan, E. (1998) Electrochemical properties of polyoxometalates as electrocatalysts. *Chem. Rev. (Washington, D.C.)*, 98: 219–237.
19. Weinstock, I.A. (1998) Homogeneous-phase electron-transfer reactions of polyoxometalates. *Chem. Rev.*, 98: 113–170.
20. See Special Issue of Appl. Catal. A-Gen., 2003, 256 on Heteropoly Acids.
21. Antonio, M.R.; Chiang, M.H.; Seifert, S.; Tiede, D.M.; Thiyagarajan, P. (2009) In situ measurement of the Preyssler polyoxometalate morphology upon electrochemical reduction: A redox system with Born electrostatic ion solvation behavior. *J. Electroanal. Chem.*, 626: 103–110.
22. Antonio, M.R.; Nyman, M.; Anderson, T.M. (2009) Direct observation of contact ion-pair formation in aqueous solution. *Angew. Chem., Int. Ed.*, 48: 6136–6140.
23. Pigga, J.M.; Kistler, M.L.; Shew, C.-Y.; Antonio, M.R.; Liu, T. (2009) Counterion distribution around hydrophilic molecular macroanions: The source of the attractive force in self-assembly. *Angew. Chem., Int. Ed.*, 48: 6538–6542.
24. Brown, G.M.; Noe-spirlet, M.R.; Busing, W.R.; Levy, H.A. (1977) Dodecatungstophosphoric acid hexahydrate, $(H_5O_2^+)_3(PW_{12}O_{40}^{3-})$. The true structure of Keggin's ''pentahydrate'' from single-crystal X-ray and neutron-diffraction data. *Acta Crystallogr. Sect. B-Struct. Commun.*, 33: 1038–1046.
25. Keggin, J.F. (1934) Structure and formula of 12-phosphotungstic acid. *Proc. Roy. Soc. (London)*, A144: 75–100.
26. Pope, M.T. (1983) *Heteropoly and Isopoly Oxometalates*; Springer-Verlag: Berlin.
27. Pope, M.T. (2004) Polyoxoanions: Synthesis and structure. In: *Applications of Coordination Chemistry*, Ward, M., ed., Elsevier: Oxford, 635–678.
28. Smit, J.V.R. (1991) Insoluble heteropolyacid salts. In: *Inorganic Ion Exchangers in Chemical Analysis*, Qureshi, M.; Varshney, K.G., eds.; CRC Press: Boca Raton, FL, 57–90.
29. Coetzee, C.J. (1991). Inorganic ion exchangers for ion-selective electrodes. In: *Inorganic Ion Exchangers in Chemical Analysis*, Qureshi, M.; Varshney, K.G., eds.; CRC Press: Boca Raton, FL, 143–175.

30. Ganapathy, S.; Fournier, M.; Paul, J.F.; Delevoye, L.; Guelton, M.; Amoureux, J.P. (2002) Location of protons in anhydrous Keggin heteropolyacids $H_3PMo_{12}O_{40}$ and $H_3PW_{12}O_{40}$ by $^1H\{^{31}P\}/^{31}P\{^1H\}$ REDOR NMR and DFT quantum chemical calculations. *J. Am. Chem. Soc.*, 124: 7821–7828.
31. Kozhevnikov, I.V.; Sinnema, A.; Vanbekkum, H. (1995) Proton sites in Keggin heteropoly acids from ^{17}O NMR. *Catal. Lett.*, 34: 213–221.
32. Farcasiu, D.; Li, J.Q. (1995) Acidity measurements on a heteropoly-acid hydrate in acetic-acid solution – A case of 3 hydrons ionizing independently, rather than consecutively. *J. Catal.*, 152: 198–203.
33. Yang, J.; Janik, M.J.; Ma, D.; Zheng, A.M.; Zhang, M.J.; Neurock, M.; Davis, R.J.; Ye, C.H.; Deng, F. (2005) Location, acid strength, and mobility of the acidic protons in Keggin 12-$H_3PW_{12}O_{40}$: A combined solid-state NMR spectroscopy and DFT quantum chemical calculation study. *J. Am. Chem. Soc.*, 127: 18274–18280.
34. Macht, J.; Carr, R.T.; Iglesia, E. (2009) Functional assessment of the strength of solid acid catalysts. *J. Catal.*, 264: 54–66.
35. Reddy, K.M.; Lingaiah, N.; Prasad, P.S.S.; Suryanarayana, I. (2006) Acidity constants of supported salts of heteropoly acids using a methodology related to the potentiometric mass titration technique. *J. Solution Chem.*, 35: 407–423.
36. Lakshmanan, V.I.; Haldar, B.C. (1969) Extractive behavior of 12-heteropoly acids. I. Extraction of 12-tungstophosphoric acid. *J. Indian Chem. Soc.*, 46: 512–524.
37. Lakshmanan, V.I.; Haldar, B.C. (1970) Extractive behavior of 12-heteropoly acids. II. Extraction of 12-molybdophosphoric, 12-tungstosilicic, and 12-molybdosilicic acids. *J. Indian Chem. Soc.*, 47: 231–238.
38. Lakshmanan, V.I.; Haldar, B.C. (1970) Extractive behavior of 12-heteropoly acids. III. Extraction of 12-tungstophosphoric, 12-molybdophosphoric, 12-tungstosilicic, and 12-molybdosilicic acids by TBP in organic diluents. *J. Indian Chem. Soc.*, 47: 72–78.
39. Asakura, T.; Donnet, L.; Picart, S.; Adnet, J.M. (2000) Extraction of hetero polyanions, $P_2W_{17}O_{61}^{10-}$, $P_2W_{18}O_{62}^{6-}$, $SiW_{11}O_{39}^{8-}$ by TBP. *J. Radioanal. Nucl. Chem.*, 246: 651–656.
40. Himeno, S.; Takamoto, M.; Ueda, T. (2005) Formation of α- and β-Keggin-type $[PW_{12}O_{40}]^{3-}$ complexes in aqueous media. *Bull. Chem. Soc. Jpn.*, 78: 1463–1468.
41. Zhu, Z.; Ruan, T.; Rhodes, C. (2003) A study of the decomposition behavior of 12-tungstophosphate heteropolyacid in solution. *Can. J. Chem.*, 81: 1044–1050.
42. Horwitz, E.P.; Dietz, M.L.; Chiarizia, R.; Diamond, H.; Essling, A.M.; Graczyk, D. (1992) Separation and preconcentration of uranium from acidic media by extraction chromatography. *Anal. Chim. Acta*, 266: 25–37.
43. Thiyagarajan, P.; Epperson, J.E.; Crawford, R.K.; Carpenter, J.M.; Klippert, T.E.; Wozniak, D.G. (1997) The time-of-flight small-angle neutron diffractometer (SAD) at IPNS, Argonne National Laboratory. *J. Appl. Crystallogr.*, 30: 280–293.
44. Pedersen, J.S. (1997) Analysis of small-angle scattering data from colloids and polymer solutions: Modeling and least-squares fitting. *Adv. Colloid Interface Sci.*, 70: 171–210.
45. Baxter, R.J. (1968) Percus-Yevick equation of hard spheres with surface adhesion. *J. Chem. Phys.*, 49: 2770–2774.
46. Goyal, P.S.; Menon, S.V.G.; Dasannacharya, B.A.; Thiyagarajan, P. (1995) Small-angle neutron-scattering study of micellar structure and interparticle interactions in Triton X-100 Solutions. *Phys. Rev. E*, 51: 2308–2315.
47. Menon, S.V.G.; Kelkar, V.K.; Manohar, C. (1991) Application of Baxter model to the theory of cloud points of nonionic surfactant solutions. *Phys. Rev. A*, 43: 1130–1133.
48. Hiemenz, P.C.; Rajagopalan, R. (Eds.) (1997) *Principles of Colloid and Surface Chemistry*; Marcel Dekker, New York.
49. Nisar, A.; Zhuang, J.; Wang, X. (2009) Cluster-based self-assembly: Reversible formation of polyoxometalate nanocones and nanotubes. *Chem. Mat.*, 21: 3745–3751.
50. Nyman, M.; Rodriguez, M.A.; Anderson, T.M.; Ingersoll, D. (2009) Two structures toward understanding evolution from surfactant-polyoxometalate lamellae to surfactant-encapsulated polyoxometalates. *Cryst. Growth Des.*, 9: 3590–3597.
51. Yin, S.Y.; Li, W.; Wang, J.F.; Wu, L.X. (2008) Mesomorphic structures of protonated surfactant-encapsulated polyoxometalate complexes. *J. Phys. Chem. B*, 112: 3983–3988.
52. Li, H.L.; Sun, H.; Qi, W.; Xu, M.; Wu, L.X. (2007) Onionlike hybrid assemblies based on surfactant-encapsulated polyoxometalates. *Angew. Chem., Int. Ed.*, 46: 1300–1303.
53. Li, W.; Bu, W.F.; Li, H.L.; Wu, L.X.; Li, M. (2005) A surfactant-encapsulated polyoxometalate complex towards a thermotropic liquid crystal. *Chem. Commun.*, 10: 3785–3787.
54. Li, C.; Jiang, Z.X.; Gao, J.B.; Yang, Y.X.; Wang, S.J.; Tian, F.P.; Sun, F.X.; Sun, X.P.; Ying, P.L.; Han, C.R. (2004) Ultra-deep desulfurization of diesel: Oxidation with a recoverable catalyst assembled in emulsion. *Chem.-Eur. J.*, 10: 2277–2280.
55. Kurth, D.G.; Lehmann, P.; Volkmer, D.; Muller, A.; Schwahn, D. (2000) Biologically inspired polyoxometalate-surfactant composite materials. Investigations on the structures of discrete, surfactant-encapsulated clusters, monolayers, and Langmuir-Blodgett films of $(DODA)_{40}(NH_4)_2[(H_2O)_n \subset Mo_{132}O_{372}(CH_3CO_2)_{30}(H_2O)_{72}]$. *J. Chem. Soc.-Dalton Trans.*, 21: 3989–3998.
56. Kurth, D.G.; Lehmann, P.; Volkmer, D.; Colfen, H.; Koop, M.J.; Muller, A.; Du Chesne, A. (2000) Surfactant-encapsulated clusters (SECs): $(DODA)_{20}(NH_4)[H_3Mo_{57}V_6(NO)_6O_{183}(H_2O)_{18}]$, a case study. *Chem.-Eur. J.*, 6: 385–393.